# Soft Matter

Volume 1 | Number 1 | Jan 2013 | Pages 1–100

## Soft Matter

www.rsc.org/softmatter

ROYAL SOCIETY
OF CHEMISTRY

www.rsc.org/softmatter

# Soft Matter

## ARTICLE

# Hierarchical Superstructures from A Star-shaped Molecule Consisted of A Cyclic Oligosiloxane with Cyanobiphenyl Moieties

Dae-Yoon Kim,[a] Minwook Park,[a] Sang-A Lee,[a] Soeun Kim,[a] Chih-Hao Hsu,[b] Namil Kim[c] Shiao-Wei Kuo,[d] Tae-Ho Yoon,[e] and Kwang-Un Jeong*[a]

Unconventional star-shaped liquid crystals (abbreviated as SiLC) were successfully synthesized by chemically connecting four cyanobiphenyl anisotropic mesogens to the periphery of a super-hydrophobic and ultra-flexible cyclic tetramethyltetrasiloxane ring with flexible hexyl chains. Based on the combined experimental techniques of differential scanning calorimetry (DSC), cross-polarized optical microscopy (POM), solid-state carbon-13 ($^{13}$C) nuclear magnetic resonance (NMR) spectroscopy and one-dimensional (1D) wide-angle x-ray diffraction (WAXD), it was found that SiLC molecule exhibited the monotropic phase transition from a LC phase to a crystalline phase. Crystalline phase was only detected during slow heating processes above its glass transition temperature, while a LC phase is formed both during cooling and during heating processes. The hierarchical superstructures were identified from the structure-sensitive 2D WAXD of the macroscopically oriented SiLC film and confirmed by selected area electron diffraction (SAED) of the SiLC single crystals. The molecular packing symmetry in the monoclinic unit cell was further investigated by computer simulations on the real and reciprocal spaces. Macroscopically oriented SiLC hierarchical superstructures on the different length scales may provide the targeted physical properties, which can allow us to apply SiLC molecules in the fields of electro-optical devices and nonlinear optics.

## 1. Introduction

Molecular self-assembly is a fundamental bottom-up principle to build up the hierarchical systems along with the possible involvement of growth kinetics.[1] Formation of hierarchical superstructures from noncovalent interactions of nucleic acids on the different length scales or host-guest interactions of cycloamyloses with macromolecules can be representative examples of the self-assembled bottom-up method found in nature.[2] Since the first discovery of liquid crystal (LC) materials in the 1880s, LC has been considered as the promising building block molecule in the bottom-up method. The science and engineering of LC have significantly contributed to the fundamental understandings and developments of the partially ordered soft materials and their self-assembled superstructures.[3] Due to the anisotropic physical properties combined with the self-healing effects, LC materials play a key role in determining the electrical and optical performances of the LC devices.[4]

Since the anisotropic physical properties of LC materials are intrinsically originated from the anisotropic molecular shapes, the conventional LC compounds consist of a calamitic and/or discotic rigid core and flexible alkyl or alkoxy chains.[5] The property-structure relationships of the conventional LC compounds can be predicted by theoretical calculations based on the experimental data.[6] However, numerous unconventional anisotropic LC materials including polycatenar-/metallomesogen-/cyclic-compounds and swallow-/star-/banana-shaped molecules have been newly synthesized.[7]

In this circumstance, the introduction of silicon connectors into the LC compounds is attractive in the LC devices because they improve the response time under the external stimuli and the mechanical flexibility and durability.[8] Anisotropic properties of silicon-based LC materials are imparted by chemically attaching polymeric or low molar mass (LMM) materials. Since the silicon-based polymeric LC systems have some limitations such as complicated synthesis protocol and long response time to an applied field due to its high viscosity, the silicon-based oligomeric LC has been proposed.[9] The mesophase of LMM-LCs is often generated by the nanophase separation between the rigid aromatic mesogens and flexible alkyl groups.[10] Therefore, the formation of mesophase can be enhanced by incorporating the short silicon segments such as

linear oligocarbosilane, cubic oligosilsesquioxane, and cylic oligosiloxane.[11]

In this research, we newly designed and synthesized a star-shaped cyanobiphenyl-substituted cyclic silicon LC molecule (abbreviated as SiLC). A cyclic tetramethyltetrasiloxane ring was selectively chosen for the ultra-flexible and super-hydrophobic central core because the ordered structures with low viscosity are useful in LC displays, nonlinear optics, information storage, and electro-optical devices.[12] It was also possible to adjust the number of anisotropic cyanobiphenyl mesogens chemically attached to the flexible core for enhancing inter- and intra-molecular interactions. Therefore, there were two main driving forces in the formation of the ordered hierarchical superstructures in this system: the super-hydrophobic interaction among the cyclic siloxanes, and the nanophase separation between the rigid cyanobiphenyl mesogens and the flexible alkyl chains. The hierarchical superstructures and phase behaviors of SiLC were investigated by the combination of differential scanning calorimetry (DSC), one-dimensional (1D) wide-angle x-ray diffraction (WAXD), cross-polarized optical microscopy (POM), and solid-state carbon-13 ($^{13}$C) nuclear magnetic resonance (NMR) techniques. Especially, the hierarchical crystalline superstructure identified by 2D WAXD of the macroscopically oriented film was confirmed by selected area electron diffraction (SAED) of the SiLC single crystal and its molecular packing symmetry in the unit cell was further investigated by computer simulations on the real and reciprocal spaces.

## 2. Experiment

### Materials

4'-hydroxy-4-biphenylcarbonitrile (CBP, 97%, Aldrich), 2,4,6,8-tetramethylcyclotetrasiloxane (TMCTS, 95%, TCI), 6-bromo-1-hexene (95%, TCI), platinum(0)-1,3-divinyl-1,1,3,3-tetramethyldisiloxane (Karstedt's catalyst, 2 wt% in xylene, Aldrich), and potassium carbonate ($K_2CO_3$, 99.99%, Aldrich) were used as-received unless otherwise noted. *N,N*-dimethylformamide (DMF, 99.8%, Sigma-Aldrich), and toluene (99.8%, Sigma-Aldrich) were distilled by conventional methods prior to use. Merck silica gel (9385 grade, 230-400 mesh) was used for all column chromatography separations.

### Synthesis

**4-cyano-4'-hex-5-en-1-oxy-biphenyl (1)**. A solution of 6-bromo-1-hexene (5 g, 30.0 mmol), 4'-hydroxy-4-biphenyl-carbonitrile (6.32 g, 32.0 mmol), and $K_2CO_3$ (5.44 g, 32.8 mmol) in 150 ml of dried DMF was refluxed for 24 h in $N_2$ atmosphere. After reaction, solvent was removed in vacuum and the residue was dissolved in chloroform and washed with distilled water several times. The organic layer was dried over $MgSO_4$. It was purified by column chromatography with silica gel using $CH_2Cl_2$:*n*-hexanes = 5:1. Resulting product was opaque white oil (Yield: 90%). $^1$H NMR (400 MHz, CDCl$_3$, TMS): δ = 1.61 (m, 2H), 1.84 (m, 2H), 2.14 (m, 2H), 4.02 (t,

2H), 5.03 (m, 2H), 5.85 (m, 1H), 6.89 (d, 2H), 7.54 (d, 2H), 7.62 (d, 2H), 7.67 ppm (d, 2H).

**SiLC (2)**. 4-cyano-4'-hex-5-en-1-oxy-biphenyl (4.71 g, 17.0 mmol) was added to a solution of 2,4,6,8-tetramethyl-cyclotetrasiloxane (1 g, 4.17 mmol) in 40 ml of toluene. The solution was allowed to stir for 30 min with nitrogen purge. Platinum(0)-1,3-divinyl-1,1,3,3-tetramethyldisiloxane (0.3 g) was added as a solution in toluene (3 ml). The reaction was heated to 100 °C and stirred for 24 h. After hydrosilation was complete, the reaction mixture was cooled to room temperature. Dissolved solution was extracted with distilled water and the dried over $MgSO_4$. It was purified by column chromatography with silica ($CH_2Cl_2$:*n*-hexanes = 5:3). Resulting product was white powder (Yield: 76.4 %). $^1$H NMR (400 MHz, CDCl$_3$, TMS): δ = 0.08 (s, 12H), 0.55 (t, 8H), 1.40 (m, 24H), 1.79 (m, 8H), 3.98 (t, 8H), 6.96 (m, 8H), 7.49 (m, 8H), 7.60 (m, 8H), 7.67 ppm (m, 8H); $^{13}$C NMR (400 MHz, CDCl$_3$, TMS): δ = 0.57, 17.1, 22.9, 25.8, 29.1, 32.8, 68.1, 110.0, 115.0, 119.0, 126.9, 128.2, 131.2, 132.5, 145.1, 159.7 ppm.

### Equipment and Experiments

Phase transition behavior of SiLC was studied using a Perkin-Elmer PYRIS Diamond DSC with an Intracooler 2P apparatus. The temperatures and heat flows were calibrated using indium and zinc standards at cooling and heating rates ranging from 2.5 to 40 °C min$^{-1}$. Heating experiments always preceded the cooling experiments at the same scanning rate in order to eliminate previous thermal histories. The transition temperatures were determined by measuring the onset temperatures from both the cooling and heating scans at different rates. Optical textures of the ordered phases were observed with POM (Nikon ECLIPSE E600POL) coupled with a LINKAM LTS 350 heating stage in order to investigate morphology on the micrometer scale.

1D WAXD experiments were conducted in the reflection mode of a Rigaku 12 kW rotating-anode x-ray (Cu K$_\alpha$ radiation) generator coupled with a diffractometer. The position and width of diffraction peaks were calibrated with silicon crystals in the high 2θ-angle region (>15°) and silver behenate in the low 2θ-angle region. To monitor the structural evolutions with temperature changes, a hot stage calibrated to be within ±1 °C error was coupled to the diffractometer. Samples were scanned across a 2θ-angle range of 1.5° to 35° at a scanning rate of 10° min$^{-1}$.

The oriented 2D WAXD patterns were obtained using a Rigaku x-ray imaging system with an 18 kW rotating anode x-ray generator. The diffraction peak positions and widths were also calibrated with silicon crystals and silver behenate. A hot stage was employed to obtain diffraction peaks at elevated temperatures. At least 30 min exposure time was required for a high-quality pattern. In 2D WAXD experiments, background scattering was subtracted from the sample scans.

Bright-field TEM images (FEI Tecnai 12) were taken to examine the film morphology on the nanometer length scale at an accelerating voltage of 120 kV. The camera length for selected area electron diffraction (SAED) analysis was set at

3.0 m, and the calibration of the SAED spacing smaller than 0.384 nm was carried out using evaporated thallous chloride, which has a largest first-order spacing diffraction of 0.384 nm. Spacing values larger than 0.384 nm were calibrated by doubling the d-spacing values of the first order diffractions.

Conformational changes of the alkyl chain in SiLC at different temperatures were also studied using solid-state ^{13}C NMR spectroscopy (Chemagnetics CMX 200) operating at 201.13 and 50.78 MHz for ^{13}C nuclei, respectively. The samples were spun in nitrogen gas at 4.5 kHz at the magic angle. The magic angle was optimized by the intensity calibration of the aromatic carbon resonance of hexamethylbenzene. The ^{13}C NMR spectra with CP/MAS/DD were acquired to selectively investigate the rigid components, and the Bloch decay spectra with MAS/DD were used to particularly study the mobile components. The CP contact time was 1 ms, while the recycle time of the pulse was 5 s. Each spectrum consisted of an accumulation of 500 scans. The temperature of the solid-state ^{13}C NMR experiment was controlled using a REX-F900 VT unit. Overlapped carbon peaks in solid-state ^{13}C NMR were resolved using the PeakFit peak separation program from Jandel Scientific. Lorentzian functions were used to obtain the best reasonable fit.

Crystallographic simulation was performed using Cerius[2] (Version 4.6) simulation software from Accelrys utilizing the COMPASS force field. The global equilibrium conformation of the SiLC compound in the isolated gas phase was chosen as the starting building block. Basic unit cell parameters determined by crystallographic experimental data from 2D WAXD of the macroscopically oriented SiLC film and SAED of SiLC single crystals were used to build the crystal unit cell. The molecular packing symmetry in this unit cell was judged by comparing the calculated diffraction patterns with those of experiments.

## 3. Results and discussion

### Programmed Star-shaped Oligosiloxane LC Molecule

A cyclic silicon-based LC molecule (abbreviated as SiLC) containing four cyanobiphenyl moieties is newly designed and synthesized, as illustrated in Fig. 1. By precisely locating the flexible alkyl connectors to the rigid cyanobiphenyl mesogens at the periphery of super-hydrophobic and ultra-flexible cyclic siloxane ring, the nanophase separation between cyanobiphenyl mesogens and cyclic siloxanes is maximized. From a synthetic point of view, the 2,4,6,8-tetramethylcyclotetrasiloxane (TMCTS) cyclic ring containing four Si-H functions allows us to synthesize a discrete and well-defined SiLC compound by a click chemistry.

As shown in Scheme 1, the olefin terminated alkyl ether of 4'-hydroxy-4-biphenyl-carbonitrile is first prepared from the corresponding bromide compound with potassium carbonate and then the cyanobiphenyl substituted cyclic oligomeric siloxane was synthesized by the hydrosilation of olefin terminated cyanobiphenyl mesogens with a multi-functional cyclic hydrosiloxane TMCTS. The reaction is conducted in the presence of a Pt(0) catalyst, divinyl(tetramethyldisiloxane)

platinum.[13] The detailed synthetic procedures are described in the experimental section of this paper. Chemical structures and purities of SiLC and its intermediates are confirmed by ^{1}H NMR (see Fig. S1 and S2 in the Supporting Information), ^{13}C NMR (Fig. S3), and thin layer chromatography (TLC).
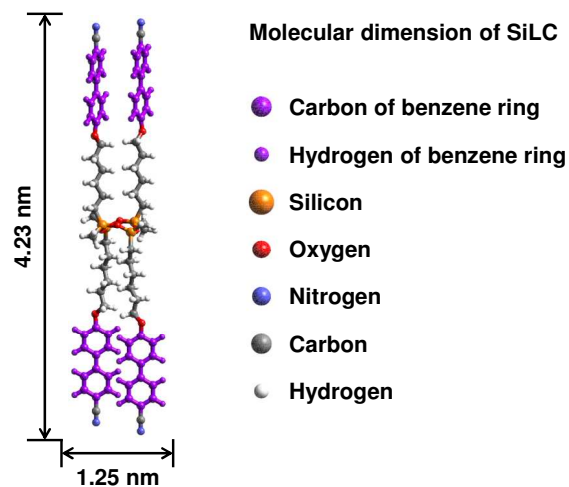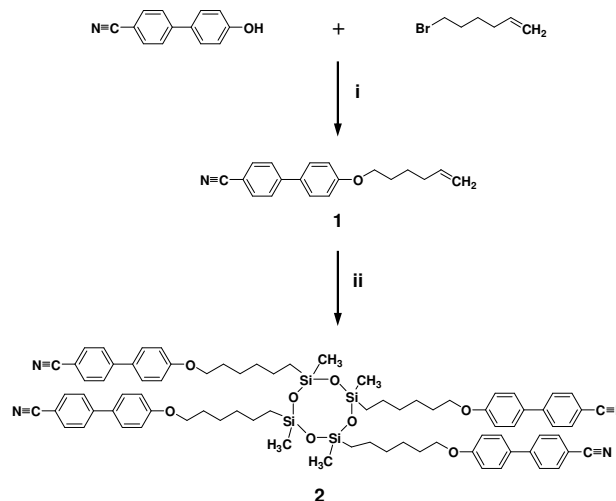


Fig. 1 Chemical structure and calculated geometric dimensions of the SiLC.



Scheme 1 Synthesis of SiLC. Reagents and conditions: i) CBP, bromohexane, K$_2$CO$_3$, DMF, 90 °C, 24 h; ii) Karstedt's catalyst, TMCTS, toluene, 100 °C, 24 h.

The molecular weight of SiLC is 1349.9 g mol^{-1}. The molecular dimensions and energy-minimized geometry in the isolated gas phase are estimated by performing computer simulation. As represented in Fig. 1, two cyanobiphenyl mesogens connected at 1 and 3 positions of cyclic siloxane with hexyl chains are located at one side of cyclic siloxane, while the other two cyanobiphenyl mesogens at 2 and 4 positions are located at the other side. Therefore, the overall shape of SiLC compound is ribbon-like. From the all-trans conformation in the alkyl chains, the calculated length of SiLC is 4.23 nm, while the width of the SiLC along the short axis is 1.25 nm, as illustrated in Fig. 1.

## Thermodynamic Phase Transitions and Their Corresponding Structural Evolutions

DSC experiment was first conducted at cooling and heating rates ranging from 2.5 to 40 °C min^{-1} to determine the thermal transition temperatures and quantitative thermodynamic properties of the SiLC compound. As shown in Fig. 2, a single exothermic first-order thermal transition is observed at 119 °C with -7.34 J g^{-1} (-9.91 kJ mol^{-1}) during a rapid cooling at 40.0 °C min^{-1}. Upon further cooling, a sudden step change of heat capacity is detected at 22 °C, which is attributed to the glass transition temperature ($T_g$) of SiLC. DSC thermogram obtained upon subsequent heating at 40 °C min^{-1} exhibits strong endothermic first-order transition at 119 °C with 7.35 J g^{-1} (9.92 kJ mol^{-1}). Similar thermal transition behaviors are observed at the scanning rates of 10 to 40 °C min^{-1}.
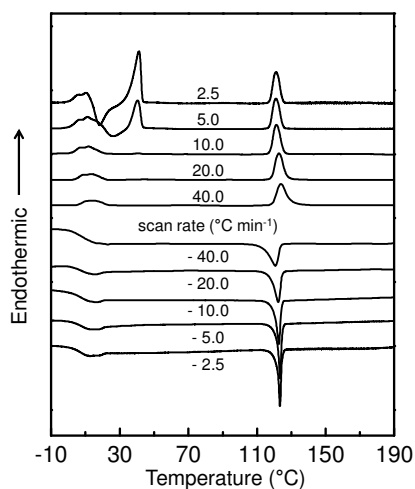


Fig. 2 Sets of DSC cooling and subsequent heating thermal diagrams of SiLC molecule at scanning rates ranging from 2.5 to 40 °C min^{-1}.

When the scanning rate is reduced to 5.0 and 2.5 °C min^{-1}, on the other hand, exothermic and endothermic thermal transitions are newly observed slightly above the $T_g$. Relatively larger heat is evolved at a slower heating rate: -10.85 J g^{-1} (-14.64 kJ mol^{-1}) for 2.5 °C min^{-1}) and -3.72 J g^{-1} (-5.02 kJ mol^{-1}) for the 5.0 °C min^{-1}. Since the amount of heat released during the exothermic transition is almost identical to that of heat absorbed during the endothermic transition, the exothermic transition can be due to the recrystallization of SiLC. The onset temperature and corresponding heat at 119 °C show no change regardless of cooling and heating rate because the first-order thermal transition is close to the equilibrium state. From the POM analysis, it is found that the transition at elevated temperature is associated with liquid crystal (LC)-isotropic melt (I) transition of SiLC.[14] The fast cooled SiLC reveals a glassy LC phase below $T_g$ = 22 °C.

Although DSC experiments are sensitive to heat absorption and release events, this technique cannot provide direct information about structural changes.[15] The 1D WAXD experiments at different temperatures are combined with DSC results to identify the corresponding structure evolutions. Fig. 3

shows a set of 1D WAXD powder patterns obtained at cooling and subsequent heating rate of 2.5 °C min^{-1}. It is realized that SiLC undergoes the isotropization above $T_i$ = 119 °C, exhibiting three amorphous scatterings at $2\theta$ = 2.91° (d = 3.03 nm), $2\theta$ = 12.01° (d = 0.74 nm) and $2\theta$ = 19.59 ° (d = 0.45 nm). The amorphous halo at $2\theta$ = 2.91° corresponds to the average periodicity of electron density fluctuations between the nanophase separated cyclic siloxane cores and cyanobiphenyl mesogens while the amorphous halo at $2\theta$ = 19.59° and at $2\theta$ = 12.01° comes from the average distances between the cyanobiphenyl mesogens and between the cyclic siloxane cores, respectively. It is apparent that the nanophase separation between cyanobiphenyl mesogens and cyclic siloxanes is maintained even in the isotropic (I) phase by locating the flexible alkyl connectors to the rigid cyanobiphenyl mesogens at the periphery of super-hydrophobic and ultra-flexible cyclic siloxane. When the temperature is decreased below $T_i$ = 119 °C, the scattering halo at $2\theta$ = 19.59° (d-spacing = 0.45 nm) suddenly shifts to $2\theta$ = 20.84° (d-spacing = 0.42 nm) with a smaller width at half height. At a low-angle region, a single strong diffraction peak at $2\theta$ = 2.91° (d = 3.03 nm) is concurrently emerged but its high-order diffractions are very weak. However, the amorphous halo at $2\theta$ = 12.01° is not much changed. As further cooling below $T_g$ = 22 °C, the 1D WAXD patterns are not changed. Based on the 1D WAXD data combined with DSC results, it is clear that a low-ordered smectic LC phase is formed by the self-organization of rigid cyanobiphenyl mesogens in the nanophase separated domains below $T_i$ = 119 °C and the molecular packing symmetry is still retained below $T_g$ = 22 °C. Therefore, the structure below $T_g$ = 22 °C should be denoted as a metastable glassy smectic LC phase.
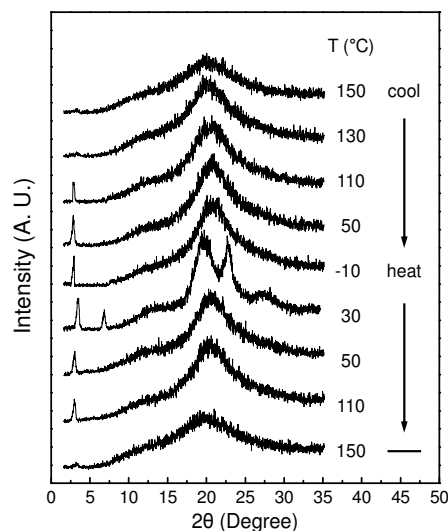


Fig. 3 A set of 1D WAXD powder patterns of SiLC molecule obtained at different temperature between -10 and 150 °C during cooling and subsequent heating at a rate of 2.5 °C min^{-1}.

As subsequently heating above the $T_g$ of SiLC molecule at a rate of 2.5 °C min^{-1}, several sharp reflection peaks suddenly

appear in both low and wide-angle regions due to the development of highly ordered crystals. Phase transition at 30 °C should be closely associated with the exothermic thermal transition detected between $T_g$ and 35 °C in DSC results (Fig. 2). The sharp diffraction peak at 2θ = 2.91° (d = 3.03 nm) shifts to 2θ = 3.39° (d = 2.60 nm) and its second-order diffraction peak is also observed at 2θ = 6.78° (d = 1.30 nm). In the wide-angle region, the scattering halo at 2θ = 20.84° (d-spacing = 0.42 nm) at the glassy smectic LC phase is split to three distinct diffraction peaks at 2θ = 19.59°, 22.74° and 27.24°, which correspond to the d-spacings of 0.45 nm, 0.39 nm and 0.32 nm, respectively. The diffraction peaks at wide-angle regions are mainly related to the lateral molecular packing between cyanobiphenyl mesogens. However, the amorphous halo at 2θ = 12.01° detected in the smectic LC phase is not much changed even in the crystalline phase. This result refers to the fact that the nanophase separated cyclic siloxane groups are in a disordered state with a short-range positional order even in the crystalline phase. The 1D WAXD pattern at 30 °C clearly indicates that the constructed hierarchical crystalline SiLC superstructure is a layered structure. However, its molecular packing symmetry in the smectic layer should be identified by 2D WAXD of oriented sample, which will be discussed in this paper. When the temperature is increased above the endothermic transition at 35 °C, the SiLC crystal phase transforms to a smectic LC phase. This explanation is justified by the fact that the 1D WAXD patterns at 50 °C obtained during cooling and subsequent heating processes are almost identical. Above $T_i$ = 119 °C, a typical 1D WAXD pattern for the I phase is observed.
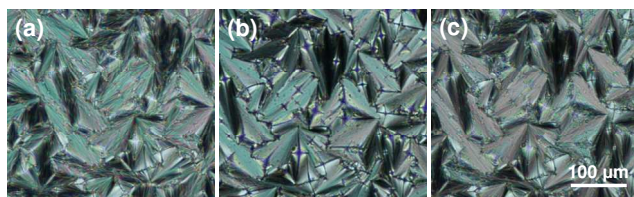


Fig. 4 POM images of SiLC molecule at (a) -10 °C, (b) 30 °C and (c) 50 °C during heating at 2.5 °C min⁻¹.

Phase transformations from the I phase to the smectic LC phase and the crystalline K phase can be further supported by the morphological investigation on the micrometer length scale. Optical textures of SiLC upon cooling and subsequent heating at 2.5 °C min⁻¹ from -10 °C to 130 °C have been recorded, and textures at -10 °C, 30 °C and 50 °C are represented in Fig. 4a, 4b and 4c, respectively. As cooling below $T_i$, the fan-shaped textures are grown against the dark state, suggestive of the emergence of a low-ordered smectic LC phase.[16] As shown in Fig. 4a, the fully grown fan-shaped textures are still discernible even below $T_g$, which agrees well with DSC and 1D WAXD results. Upon heating at 2.5 °C min⁻¹ above $T_g$, the boundary lines between the fan-shaped domains and the Maltese cross in each fan-shape domain get obvious, as shown in Fig. 4b, which phenomena are often detected during a recrystallization process.

The fan-shaped texture observed during cooling appears again above 35 °C due to the K→LC transition (Fig. 4c).
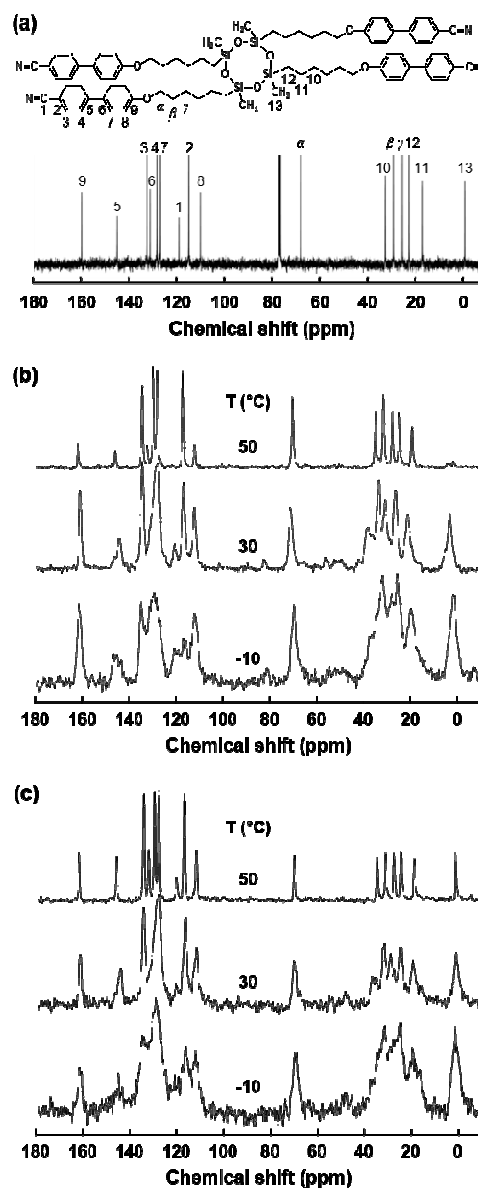


Fig. 5 Solution ¹³C NMR spectrum of SiLC molecule (a) and sets of solid-state ¹³C NMR spectra of SiLC molecule during heating between -10 °C to 50 °C: CP/MAS/DD method (b) and Bloch decay method (c).

From the combined experiments of DSC, 1D WAXD and POM, it is realized that there are two stable hierarchical superstructures of SiLC molecule depending on temperature: one is a low-ordered smectic LC phase at high temperature and the other is a crystalline structure formed by annealing a metastable glassy smectic LC phase above $T_g$. Note that the cyclic siloxane group of SiLC molecule is involved in constructing the hierarchical superstructures but the nanophase separated cyclic siloxane groups are in a disordered state with a short-range positional order even in the crystalline phase. It means that the cyclic siloxane groups of SiLC are in the mobile and flexible states in all hierarchical superstructures. To

confirm this statement, the solid-state $^{13}C$ NMR spectra with Cross Polarization/Magic Angle Spinning/Dipolar Decoupling (CP/MAS/DD) (Fig. 5b) and Bloch decay (Fig. 5c) are acquired at different temperatures to selectively investigate the rigid and mobile components of SiLC at different phases, respectively.[17]

At first, chemical shift is identified by analyzing the solution $^{13}C$ NMR. As indicated in Fig. 5a, the carbon atoms in cyanobiphenyl groups appear between 100 ppm and 170 ppm, while carbons in the alkyl chains are chemically shifted between 100 ppm and 10 ppm. Specifically, chemical shift of carbons in the cyclic siloxane ring is detected at 0 ppm. As we expected from the DSC and 1D WAXD results, the mobilities of cyclic siloxane ring and alkyl chains as well as cyanobiphenyl groups in the low-ordered smectic LC phase (50 °C) are much higher than those of the glassy smectic LC phase (-10 °C). Especially, the cyclic siloxane rings in the crystalline phase are still mobile even though the rigidity is higher than that in the low-ordered smectic LC phase. This results is well matched with those of 1D WAXD. In Fig. 5, the $^{13}C$ chemical shift at 63 ppm represents the carbon atoms at the $\alpha$ position, and the $\beta$ and $\gamma$ carbon atoms appeared at 34 and 24 ppm, respectively. Especially, the $\beta$ carbon chemical shift in the Bloch decay method consists of two values. The chemical shift at 34-32 ppm in the Block decay $^{13}C$ solid-state NMR spectra of SiLC (Fig. 5c) represents the methylene carbon atoms in the long trans zigzag segments of the alkyl chains, while the chemical shift at 32-30 ppm corresponds to the carbon atoms in the disordered, statistically distributed trans and gauche conformations. Upon increasing temperature from -10 °C (a glassy smectic LC phase) to 30 °C (a crystalline phase), the area of $\beta$ peak at 33 ppm corresponding to the carbon atoms in the ordered segments of alkyl chains suddenly increases from 40% to 60%. When the temperature is further increased up to 50 °C (a low-ordered smectic LC phase), the area of $\beta$ peak is abruptly decreased down to 40%. Temperature-dependent solid-state $^{13}C$ NMR results agree well with those of DSC, 1D WAXD and POM.
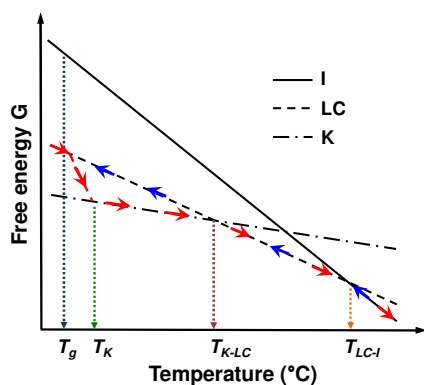


Fig. 6 Illustration of the free energy versus temperature at constant pressure for SiLC. Here, blue and red arrows represent the cooling and subsequent heating tracks, respectively.

To understand the thermodynamic phase transition behaviors of SiLC and the formation of the stable K crystalline phase, the free energy versus temperature at constant pressure is schematically illustrated based on the combined experimental data of DSC, 1D WAXD, POM and solid-state $^{13}C$ NMR. As represented as blue arrows in Fig. 6, the I phase transfers to the smectic LC phase by cooling the SiLC. Since the I ↔ LC transition is close to the equilibrium state, the transition temperature and its heat change are independent of cooling and heating rates. Upon lowering temperature below the $T_g$ of SiLC, the symmetry and order of the smectic LC phase are retained to be a glassy smectic LC phase. As illustrated in Fig. 6, as subsequently heating above the $T_g$ of SiLC, the metastable glassy smectic LC phase transforms to the stable K crystalline phase. To confirm this monotropic phase transition, SiLC compound is isothermally annealed at 30 °C right after cooling at 10 °C min$^{-1}$ using DSC. The subsequent heating at 10 °C min$^{-1}$ indicates that the crystallization starts after 10 min and finishes in 2 h. The continuous heating makes the 3D ordered crystalline K phase transformed to the smectic LC phase at $T_{K-LC}$ and to the I phase at $T_{LC-I}$. This monotropic phase transition behavior and the development of the metastable smectic LC phase below $T_K$ should be originated from the kinetic competition between the smectic LC phase and the crystalline K phase.

**Identification of Hierarchical Superstructures at Different Temperatures**

The molecular packing structures and symmetries in the hierarchical superstructures of SiLC are identified by conducting the 2D WAXD experiments. Macroscopically oriented SiLC samples for 2D WAXD experiments are first prepared by mechanical shearing at the temperature between $T_{K-LC}$ and $T_{LC-I}$ and then quenched below the $T_g$ of SiLC. The oriented and quenched sample is further annealed at the temperature between $T_g$ and $T_{K-LC}$ to prepare the macroscopically oriented K crystalline film for 2D WAXD.

A series of 2D WAXD patterns for the oriented SiLC crystal (Fig. 7d) was obtained with the incident x-ray beam directions parallel to the $x$ (Fig. 7a), the $y$ (Fig. 7b) and the $z$ (Fig. 7c) axes, respectively. Diffraction arc positions and widths in Fig. 7 are calibrated based on the diffraction ring of silicon power crystal at $2\theta = 28.466°$ (d = 0.314 nm). As discussed in 1D WAXD (Fig. 3), diffraction information about SiLC molecular arrangements appears on two different length scales. One is on the nanometer length scale in the low $2\theta$-angle region between 1.5° and 11°, which is related with hierarchical superstructures of SiLC. Diffractions on the sub-nanometer length scale between 11° and 30° can provide information about the lateral molecular packing structures between the nanophase separated cyclic siloxane cores and between the cyanobiphenyl mesogens. As represented in Fig. 7, the x-ray patterns along the $x$ and $y$ axes are identical while the 2D WAXD along the $z$ axis (Fig. 7c) shows disoriented ring patterns at wide-angle regions without any detectable diffractions at low-angle regions. Therefore, it is safe to conclude that 2D WAXD along the $x$ and $y$ axes is a uniaxially oriented fiber pattern, in which the molecular long axis is parallel to the $z$ axis (perpendicular to the

shear direction, SD). In Fig. 7a and 7b, a pair of strong diffraction at $2\theta = 3.39°$ (d = 2.60 nm) is detected on the meridian with its high order diffraction at $2\theta = 6.78°$ (d = 1.30 nm). This result indicates that the hierarchical superstructure of SiLC in the K phase is a basically layer structure with the layer d-spacing = 2.60 nm. Therefore, Miller indices of the diffractions at $2\theta = 3.39°$ and $6.78°$ are identified as (001) and (002), respectively. Note that the layer normal is parallel to the z axis which is perpendicular to the SD. Since the calculated length of SiLC is 4.23 nm (as shown in Fig. 1), SiLC molecules may overlap each other along the layer normal. On the equator of 2D WAXD along the x and y axes, three diffraction arcs are detected at $2\theta = 19.59°$ (d = 0.45 nm), $22.74°$ (d = 0.39 nm) and $27.24°$ (d = 0.32 nm) with a pair of scattering halo at $2\theta = 12.01°$ (d = 0.74 nm). Note that all diffractions and scatterings on the equator of 2D WAXD along the x and y axes appear as ring patterns in Fig. 7c (along the z axis). The scattering halo detected at $2\theta = 12.01°$ is originated from the average periodicity of electron density fluctuations between the nanophase separated cyclic siloxane cores with a short-range positional order. Since the scattering halo is detected on the equator, the layer normal of siloxane core aggregates is parallel to the z axis (meridian direction). When the molecular packing among cyanobiphenyl mesogens in the hierarchical crystalline superstructure of SiLC is only considered, three diffractions on the equator at $2\theta = 19.59°$, $22.74°$ and $27.24°$ can be assigned as the (200), (110) and (120) plane, respectively, based on the triangulation method of building a 2D $a'*b'*$ lattice of the unit cell. Through the refinement of the reciprocal 2D $a'*b'*$ lattice using the diffractions on the equator, a real space 2D unit cell is evaluated with dimensions of $a' = 0.78$ nm, $b' = 0.55$ nm, and $\gamma' = 90°$.
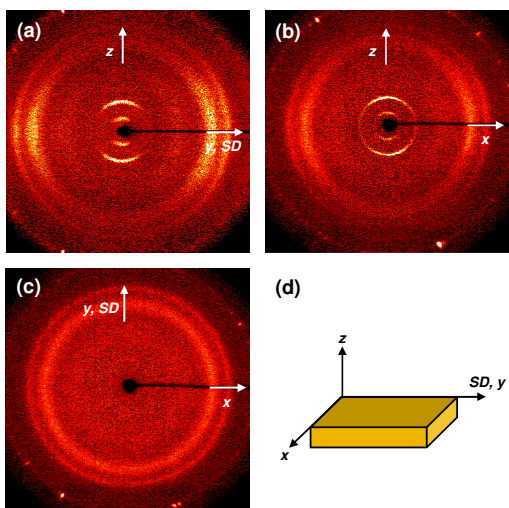


Fig. 7 2D WAXD patterns of the crystalline phase (K) of SiLC at 25 °C: the incident x-ray beam directions are parallel to the x (a), the y (b), and the z axes (c), respectively. Schematic illustration of SiLC specimen (d).

To confirm the 2D molecular packing of cyanobiphenyl mesogens in the hierarchical crystalline superstructure of SiLC, SAED experiments from single crystals are conducted. Thin

SiLC film prepared by casting the 0.05 wt% chloroform solution is cooled down to -10 °C from $T_i$ = 119 °C and subsequently heated up to 30 °C at a rate of 2.5 °C min$^{-1}$. SAED pattern of the single crystal obtained by a low dose TEM technique is shown in Fig. 8. Two pairs of electron diffractions are detected at d = 0.45 nm on the quadrants while a pair electron diffractions at d = 0.39 nm is observed on the $a'*$ axis. The (020) diffraction is also detected at d = 0.275 nm, as shown in Fig. 8. The calculated $\gamma'$-angle ($\gamma' = 90°$) based on 2D WAXD is well matched with the measured value in SAED.
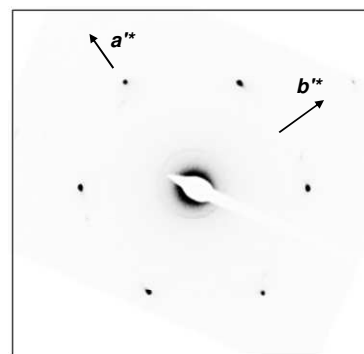


Fig. 8 SAED pattern of SiLC single crystal in the K phase.

Molecular packing structure of cyanobiphenyl mesogens in the hierarchical crystalline superstructure of SiLC determined by 2D WAXD and SAED is further verified by a computer simulation. At first, we only take care of the molecular packing of cyanobiphenyl mesogenic parts in SiLC molecules. As shown in Fig. 9, four cyanobiphenyl mesogens located at the corner are arranged along the $c'$ axis (long axis of the molecule, z axis) while the cyanobiphenyl mesogen at the center is pointing the opposite direction. This molecular arrangement exactly satisfy the diffraction patterns of the experimentally observed 2D WAXD and SAED. Furthermore, the dipole moment induced by the individual cyanobiphenyl mesogen can be canceled out to make the system stable. Note that the cyanobiphenyl mesogen at the center and at the corners should be come from the different SiLC molecules. The unit cell created only from cyanobiphenyl mesogens can not represent the K phase, but it is considered as a sub unit cell of the hierarchical crystalline superstructure of SiLC.
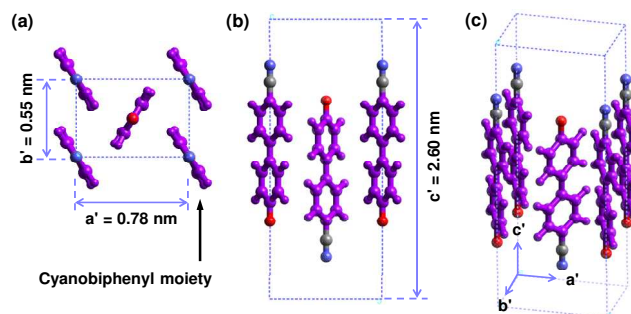


Fig. 9 Simulated molecular packing in the real space by considering only cyanobiphenyl mesogens in SiLC.

Next, to identify the hierarchical crystalline superstructure of SiLC, diffractions generated from all parts of SiLC molecule should be considered together. In Fig. 7a and 7b, the $a*$ and $b*$ axes are assigned parallel to the equator while the $c*$-axis is along the meridian direction, which is parallel to the layer normal. Based on the triangulation method of building a 2D $a*b*$ lattice of the unit cell, a scattering halo at $2\theta = 12.01°$ and three diffraction arcs at $2\theta = 19.59°$, $22.74°$ and $27.24°$ on the equator of 2D WAXD (Fig. 7a and b) can be indexed as $(1\bar{1}0)$, $(200)$, $(2\bar{2}0)$ and $(3\bar{1}0)$, respectively. Through the refinement of the reciprocal 2D $a*b*$ lattice using the diffractions on the equator, a real space 2D unit cell is evaluated with dimensions of $a = 0.95$ nm, $b = 0.95$ nm and $\gamma = 109.62°$.[18]

Table 1. Experimental and calculated crystallographic parameters of the monoclinic crystalline (K) phase of SiLC

| (hkl) | 2θ (degree) | | d-spacing (nm) | |
|---|---|---|---|---|
| | Exptl[a] | Calc[b] | Exptl[a] | Calc[b] |
| $1\bar{1}0$ | 12.01 | 11.82 | 0.74 | 0.75 |
| 200 | 19.59 | 19.65 | 0.45 | 0.45 |
| 020 | 19.59 | 19.65 | 0.45 | 0.45 |
| $2\bar{2}0$ | 22.74 | 22.85 | 0.39 | 0.39 |
| $3\bar{1}0$ | 27.24 | 27.51 | 0.32 | 0.32 |
| $1\bar{3}0$ | 27.24 | 27.51 | 0.32 | 0.32 |
| 001 | 3.39 | 3.40 | 2.60 | 2.60 |
| 002 | 6.78 | 6.80 | 1.30 | 1.30 |

[a]The accuracy of the experimental data is ±0.005 nm. [b]The calculated data listed are based on the crystalline (K) monoclinic unit cell with $a = 0.95$ nm, $b = 0.95$ nm, $c = 2.60$ nm, $\alpha = \beta = 90.0°$ and $\gamma = 109.62°$.

Since the $c*$-axis along the meridian is perpendicular to the $a*$ and $c*$ axes along the equator, both $\alpha$ and $\beta$ angles are 90°. From the strong diffraction at $2\theta = 3.39°$ with its high order diffraction at $2\theta = 6.78°$, the dimension of c-axis is determined to be 2.60 nm. Table 1 lists the experimentally observed and the calculated d-spacings based on this monoclinic unit cell lattice. With one SiLC molecule in one unit cell, its calculated crystallographic density is 1.00 g cm$^{-3}$. The experimentally observed density is 0.98 g cm$^{-3}$, which fits well with the calculated one. Therefore, this hierarchical crystalline superstructure (K) of SiLC is identified as a monoclinic crystalline phase.

The 3D molecular arrangement and packing symmetry in the monoclinic unit cell of the SiLC hierarchical crystalline superstructure are further investigated by computer simulation. The simulated molecular packing should satisfy the experimentally observed 2D WAXD and SAED results. First of all, there is a strong nanophase separation between cyanobiphenyl mesogens and cyclic siloxane groups of SiLC molecule, and four cyanobiphenyl mesogens are chemically

connected to the periphery of a cyclic siloxane ring. Second, the nanophase separated cyanobiphenyl mesogens are laterally aggregated to form the 2D orthogonal unit cell with dimensions of $a' = 0.78$ nm, $b' = 0.55$ nm, and $\gamma' = 90°$. Here, note that the cyanobiphenyl mesogens on the (11) 2D plane in the sub unit cell are all arranged parallel to the layer normal but their polar axes are opposite to the neighboring ones, as shown in Fig. 9. Finally, the cyclic siloxane groups of SiLC molecule are self-assembled to form the 2D platform with the average distance among cyclic siloxane cores = 0.74 nm. Since the scattering halo from cyclic siloxane groups is detected on the equator of 2D WAXD (Fig. 7a and 7b), the 2D platform normal is parallel to the z-axis (meridian direction). Without disturbing the molecular packing symmetry of cyanobiphenyl mesogens in the 2D orthogonal unit cell, the locations of cyclic siloxane groups are first estimated by overlapping two sub unit cells, as illustrated in Fig. 10a. By connecting four cyanobiphenyl mesogens to the periphery of a cyclic siloxane ring with hexyl chains, the 3D molecular arrangements of SiLC molecule in the K phase are recognized in the real space. This simulated molecular packing model satisfy all the experimental data observed in 2D WAXD and SAED.
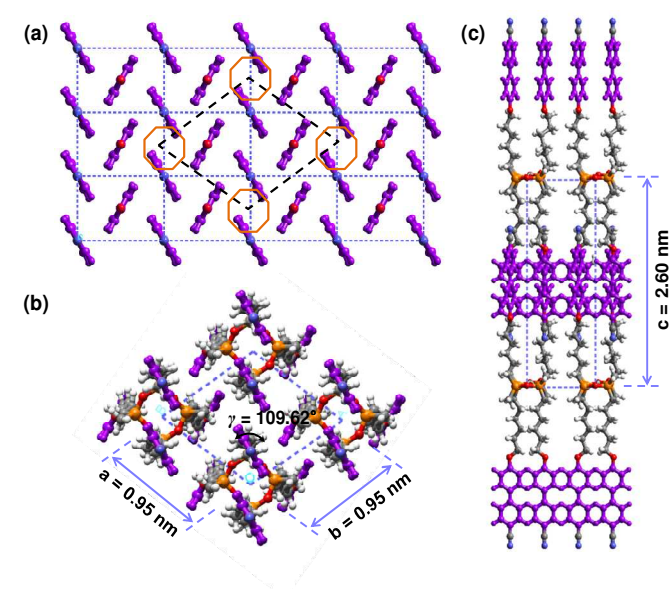


Fig. 10 Schematic illustration of the overlapping the 2D orthogonal sub unit cell of cyanobiphenyl mesogens on the 2D self-assembled SiLC platform (a). Computer simulated molecular packing in the SiLC crystal phase: [001] zone (b) and [010] zone (c).

In order to examine whether the proposed molecular packing scheme fits to the real structure, the calculated 2D WAXD and SAED diffraction patterns are generated and compared with the experimentally obtained diffraction patterns.[19] By the comparison, the precise atom positions in the monoclinic unit cell are determined. The calculated 2D WAXD fiber pattern (Fig. 11a) and SAED pattern with the [001] zone (Fig. 11b) based on the molecular packing in the real space (Fig. 10) are qualitatively matched well with the experimental observations (Fig. 7a for 2D WAXD and Fig. 8 for SAED).
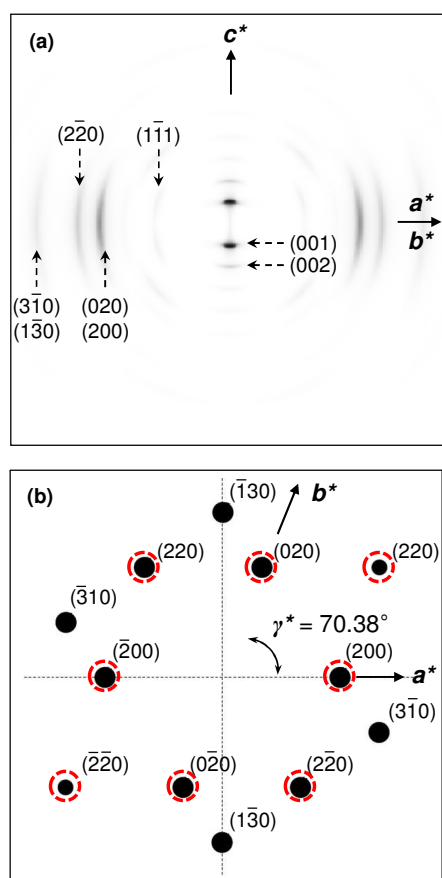
Fig. 11 Computer simulated 2D WAXD fiber pattern (a) and SAED on [001] zone (b) of SiLC in the K1 phase. The circled diffractions are experimentally observed.

The molecular packing structure of the low-ordered LC phase between $T_{K\text{-}LC}$ = 35 °C and $T_{LC\text{-}I}$ = 119 °C is also studied by the 2D WAXD patterns obtained by irradiating x-ray along the *x* (Fig. 12a), the *y* (Fig. 12b) and the *z* (Fig. 12c) axes, respectively. The 2D WAXD along the *x* and *y* axes are identical and the 2D WAXD along the *z*-axis are amorphous ring pattern without exhibiting low-angle diffractions. Similar to the 2D WAXD of K phase, the 2D WAXD of the low-ordered LC phase is a uniaxially oriented fiber pattern. As shown in Fig. 12a and 12b, a pair of diffractions is detected on the meridian at $2\theta$ = 2.91° (d = 3.03 nm) with its second order diffraction at $2\theta$ = 5.82°. This means that the hierarchical LC superstructure maintains a layer structure with d-spacing = 3.03 nm. Even though the flexible alkyl chains are assumed to be all *trans* conformation, the calculated length (4.23 nm) of SiLC is significantly bigger than the detected layer spacing (d = 3.03 nm). The smaller layer thickness compared with the length of SiLC molecule indicates the fact that the SiLC molecule is tilted with respect to layer normal or that the SiLC molecules are interdigitated with the molecules in the neighboring layers. Since the scattering halos at $2\theta$ = 20.84° (d = 0.42 nm) and $2\theta$ = 12.01° (0.74 nm) originated from the average distances between the cyanobiphenyl mesogens and between cyclic siloxane cores, respectively, are on the equator in Fig. 12a and 12b, the smectic layer should be interdigitated and the long axis of SiLC

molecule is parallel to the layer normal. Therefore, this low-ordered LC phase can be identified as a SmA phase, as schematically illustrated in Fig. 12e.
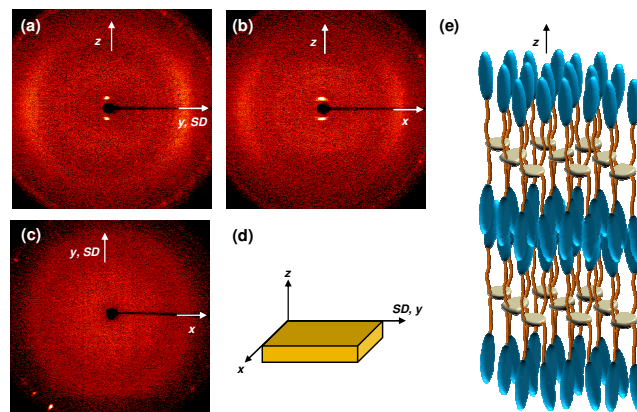


Fig. 12. 2D WAXD patterns of the liquid crystalline phase (LC) of SiLC at 70 °C: the incident x-ray beam directions are parallel to the *x* (a), the *y* (b), and the *z* axes (c), respectively. Schematic illustrations of SiLC specimen (d) and molecular packing models in the SmA LC phase (e).

## Conclusions

A star-shaped liquid crystalline (LC) molecule (abbreviated as SiLC) was newly designed and successfully synthesized by chemically connecting four cyanobiphenyl mesogens to the periphery of a cyclic tetramethyltetrasiloxane ring with flexible hexyl chains. Utilizing the combined techniques of thermal, microscopic, spectroscopic, and scattering experiments, it was found that SiLC molecule exhibited the peculiar monotropic phase transition behavior. Hierarchical crystalline (K) superstructure was only formed during heating processes above its glass transition temperature ($T_g$ = 22 °C), while the low-ordered LC phase is formed both during cooling and during heating processes. Based on the structure-sensitive 2D WAXD and SAED, the 3D hierarchical superstructures of SiLC molecule at different temperatures were identified: one is the crystalline phase with a monoclinic unit cell at low temperatures and the other is the SmA LC phase at high temperatures. The molecular packing symmetry in the hierarchical crystalline superstructure was further investigated by performing computer simulations on the real and reciprocal spaces. The hierarchical superstructures controlled on the different length scales can allow us to apply SiLC molecules in the fields of electro-optical devices and nonlinear optics.

## Acknowledgements

## Notes and references

[a] Department of Polymer-Nano Science and Technology & Polymer Materials Fusion Research Center, Chonbuk National University, Jeonju, Jeonbuk, 561-756, Korea. E-mail: kujeong@jbnu.ac.kr.

[b] Department of Polymer Science, The University of Akron, Akron, OH, 44325, USA.

[c] Smart Materials R&D Center, Korea Automotive Technology Institute, Cheonan, Chungnam 330-912, South Korea.

[d] Department of Materials Science and Optoelectronic Engineering, National Sun Yat-Sen University, Kaohsiung 804, Taiwan.

[e] Department Materials Science and Technology, Gwangju Institute of Science and Technology, Gwangju, Jeonnam 500-712, South Korea.

1   S. S. Babu, V. K. Praveen and A. Ajayaghosh *Chem. Rev.*, 2014, **114**, 1973; J. F. Stoddart, *Angew. Chem., Int. Ed.* 2012, **51**, 12902; S. Srinivasan, V. K. Praveen, R. Philip and A. Ajayaghosh *Angew. Chem., Int. Ed.*, 2008, **47**, 5750; R. J. Williams, A. M. Smith, R. Collins, N. Hodson, A. K. Das and R. V. Ulijn *Nat. Nanotechnol.*, 2009, **4**, 19; K. J. Skilling, F. Citossi, T. D. Bradshaw, M. Ashford, B. Kellam and M. Marlow *Soft Matter*, 2014, **10**, 237; J. W. Goodby, G. H. Mehl, I. M. Saez, R. P Tuffin, G. Mackenzie, R. Auzely-Velty, T. Benvegnu and D. Plusquellec *Chem. Commun.*, 1998, 2057.

2   J. Shimada, S. Handa, H. Kaneko and T. Takada *Macromolecules*, 1996, **29**, 6408; S. Honda, T. Yamamoto and Y. Tezuka *Nat. Commun.*, 2012, **4**, 1; E. A. Appel, J. Barrio, X. J. Loh and O. A. Scherman *Chem. Soc. Rev.*, 2012, **41**, 6195; J. Szejtli *Chem. Rev.*, 1998, **98**, 1743.

3   O. Z. Lehmann *Phys. Chem.*, 1888, **9**, 421; H. Kelker and P. M. Knoll *Liq. Cryst.*, 1989, **5**, 19; C. Xue, S. Jin, X. Weng, J. J. Ge, Z. Shen,; H. Shen,; M. J. Graham, K.-U. Jeong, H. Huang, D. Zhang, M. Guo, F. W. Harris and S. Z. D. Cheng *Chem. Mater.*, 2004, **16**, 1014.

4   A. Mori, M. Yokoo, M. Hashimoto, S. Ujiie, S. Diele, U. Baumeister and C. Tschierske *J. Am. Chem. Soc.*, 2003, **125**, 6620; T. Cardinaels, K. Driesen, T. N. Parac-Vogt, B. Heinrich, C. Bourgogne, D. Guillon, B. Donnio and K. Binnemans *Chem. Mater.*, 2005, **17**, 6589; S. Norvez, F.-G. Tournilhac, P. Bassoul and P. Herson *Chem. Mater.*, 2001, 13, 2552; L. Cui, J. Miao and L. Zhu *Macromolecules*, 2006, **39**, 2536; R. A. Bissell, N. Boden, R. J. Bushby, C.W. G. Fishwick, E. Holland, B. Movaghar and G. Ungar *Chem. Commun.*, **1998**, 113; J. L. Segura and N. Martin *Angew. Chem. Int. Ed.*, 2001, **40**, 1372.

5   D.-Y. Kim, L. Wang, Y. Cao, X. Yu, S. Z. D. Cheng, S.-W. Kuo, D.-H. Song, S. H. Lee, M.-H. Lee and K.-U. Jeong *J. Mater. Chem.*, 2012, **22**, 16382; S.-K. Park, S.-E. Kim, D.-Y. Kim, S.-W. Kang, S. Shin, S.-W. Kuo, S.-H. Hwang, S. H. Lee, M.-H. Lee and K.-U. Jeong *Adv. Funct. Mater.*, 2011, **21**, 2129; M.-C. Yeh, Y.-L. Su, M.-C. Tzeng, C. W. Ong, T. Kajitani, H. Enozawa, M. Takata, Y. Koizumi, A. Saeki, S. Seki and T. Fukushima *Angew. Chem. Int. Ed.*, 2013, 52, 1031.

6   N. Kim, L. Wang, D.-Y. Kim, S.-H. Hwang, S.-W. Kuo, M.-H. Lee and K.-U. Jeong *Soft Matter*, 2012, **8**, 9183; D.-Y. Kim, P. Nayek, S. Kim, K. S. Ha, M. H. Jo, C.-H. Hsu, Y. Cao, S. Z. D. Cheng, S. H. Lee and K.-U. Jeong *Cryst. Growth Des.*, 2013, **13**, 1309.

7   L. Gonzalez, N. Gimeno, R. M. Tejedor, V. Polo, M. B. Ros, S. Uriel and J. L. Serrano *Chem. Mater.*, 2013, **25**, 4503; J. Wu, T. Usui and J.-I. Hanna *J. Mater. Chem.*, 2011, **21**, 8045; R. Deschenaux, B. Donnio and D. Guillon *New. J. Chem.*, 2007, **31**, 1064; A. S. Achalkumar, U. S. Hiremath, D. S. S. Rao, C. V. Yelamaggad *Liq. Cryst.*, 2011, **38**, 1563; N. D. Suhan, S. J. Loeb and S. H. Eichhorn *J. Am. Chem. Soc.*, 2013, **135**, 400.

8   S. Rendon and W. R. Burghardt *Macromolecules*, 2007, **40**, 6624; Q. Pan, X. Chen, X. Fan, Z. Shen and Q. Zhou *J. Mater. Chem.*, 2008, **18**, 3481; X. Wang, C. M. Cho, W. Y. Say, A. Y. X. Tan, C. He, H. S. O. Chan and J. Xu *J. Mater. Chem.*, 2011, **21**, 5248; B. Donnio, S. Buathong, I. Bury and D. Guillon *Chem. Soc. Rev.*, 2007, **36**, 1495; J. T. Soltysiak, E. Bialecka-Florjanczyk and J. Przedmojski *Eur. Polym. J.*, 2006, **42**, 1662; H. Finkelmann and G. Rehage *Macromol. Chem. Rapid Commun.*, 1980, **1**, 31; K. Hiraoka, M. Kobayasi, R. Kazama and H. Finkelmann *Macromolecules*, 2009, **42**, 5600; W. Kossack, P. Papadopoulos, P. Heinze, H. Finkelmann and F. Kremer *Macromolecules*, 2010, **43**, 7532; H. Finkelmann, S. T. Kim, A. Munoz, P. Palffy-Muhoray and B. Taheri *Adv. Mater.*, 2001, *13*, 1069.

9   K. Kaneko, Y. Miwa and N. Nakamura *J. Appl. Polym. Sci.*, 2007, **105**, 2474; Z. Cheng, H. Cao, D. Zhao, W. Hu, W. He, X. Yuan, J. Xiao, H. Zhang and H. Yang *Liq. Cryst.*, 2011, **38**, 9; D. Lacey and T. E. Mann *Liq. Cryst.*, 2003, **30**, 1159; L.-M. Liu, B.-Y. Zhang, X.-Z. He and C.-S. Cheng *Liq. Cryst.*, 2004, **31**, 781; R. Zniber, R. Achour, M. Z. Cherkaoui, B. Donnio, L. Gehringer and Daniel Guillon *J. Mater. Chem.*, 2002, **12**, 2208.

10  A. S. Mocanu, M. Amela-Cortes, Y. Molard, V. Circu and S. Cordier *Chem. Commun.*, 2011, **47**, 2056; Q. Song, D. Nannenmacher, F. Giesselmann and R. P. Lemieux *J. Mater. Chem. C*, 2013, **1**, 343.

11  D.-Y. Kim, S. Kim, S.-A Lee, Y.-E. Choi, W.-J. Yoon, S.-W. Kuo, C.-H. Hsu, M.-J. Huang, S. H. Lee and K.-U. Jeong *J. Phys. Chem. C*, 2014, **118**, 6300; I. Imae and Y. Kawakami *J. Mater. Chem.*, 2005, **15**, 4581; V. V. Tsukruk, T. J. Bunning, H. Korner, C. K. Ober and W. W. Adams *Macromolecules*, 1996, **29**, 8706.

12  D. R. Medeiros, M. A. Hale, R. J. P. Hung, J. K. Leitko and C. G. Willson *J. Mater. Chem.*, 1999, **9**, 1453; C. Keith, G. Dantlgraber, R. A. Reddy, U. Baumeister, M. Prehm, H. Hahn, H. Lang and C. Tschierske *J. Mater. Chem.*, 2007, **17**, 3796.

13  A. R. Jennings and D. Y. Son *Chem. Commun.*, 2013, **49**, 3467.

14  S. Leng, B. Wex, L. H. Chan, M. J. Graham, S. Jin, A. J. Jing, K.-U. Jeong, R. M. V. Horn, B. Sun, M. Zhu, B. R. Kaafarani and S. Z. D. Cheng *J. Phys. Chem. B*, 2009, **113**, 5403; K.-U. Jeong, S. Jin, J. J. Ge, B. S. Knapp, M. J. Graham, J. Ruan, M. Guo, H. Xiong, F. W. Harris and S. Z. D. Cheng *Chem. Mater.*, 2005, **17**, 2852; A. Yamaguchi, N. Uehara, J. Yamamoto and A. Yoshizawa *Chem. Mater.*, 2007, **19**, 6455; K.-U. Jeong, D.-K. Yang, M. J. Graham, Y. Tu, S.-W. Kuo, B. S. Knapp, F. W. Harris and S. Z. D. Cheng *Adv. Mater.*, 2006, **18**, 3229; H.-J. Sun, C.-L. Wang, I-F. Hsieh, C.-H. Hsu, R. M. V. Horn, C.-C. Tsai, K.-U. Jeong, B. Lotz and S. Z. D. Cheng *Soft Matter*, 2012, **8**, 4767.

15  C. Ye, G. Xu, Z.-Q. Yu, J. W. Y. Lam, J. H. Jang, H.-L. Peng, Y.-F. Tu, Z.-F. Liu, K.-U. Jeong, S. Z. D. Cheng, E.-Q. Chen and B. Z. Tang *J. Am. Chem. Soc.*, 2005, **127**, 7668; K.-U. Jeong, B. S. Knapp, J. J. Ge, M. J. Graham, Y. Tu, S. Leng, H. Xiong, F. W. Harris and S. Z. D. Cheng *Polymer*, 2006, **47**, 3351; S. Leng, L. H. Chan, J. Jing, J. Hu, R. M. Moustafa, R. M. V. Horn, M. J. Graham, B. Sun, M. Zhu, K.-U. Jeong, B. R. Kaafarani, W. Zhang, F. W. Harris and S. Z. D. Cheng *Soft Matter*, 2010, **6**, 100.

16  I. Dierking *Textures of Liquid Crystals*, Wiley-VCH, Weinheim, 2003.

17  H. Shen, K.-U. Jeong, H. Xiong, M. J. Graham, S. Leng, J. X. Zheng, H. Huang, M. Guo, F. W. Harris and S. Z. D. Cheng *Soft Matter*, 2006, **2**, 232; S.-W. Kuo, H.-F. Lee, W.-J. Huang, K.-U. Jeong and F.-C. Chang *Macromolecules*, 2009, **42**, 1619.

18  S.-H. Hwang, S.-J. Park, H.-Y. Kim, S.-W. Kuo, S. H. Lee, M.-H. Lee and K.-U. Jeong *J. Phys. Chem. B*, 2009, *113*, 5843.

19  Y.-F. Huang, Y.-W. Chian, J. Ruan, S. Jin, K.-U. Jeong, H.-Y. Tang and A.-C. Su *Polymer,* 2011, **52**, 4114.

## Table of Content (TOC) of

**"**Hierarchical Superstructures from A Star-shaped Molecule Consisted of A Cyclic Oligosiloxane with Cyanobiphenyl Moieties**"**

Dae-Yoon Kim, Minwook Park, Sang-A Lee, Soeun Kim, Chih-Hao Hsu, Namil Kim Shiao-Wei Kuo, Tae-Ho Yoon and Kwang-Un Jeong*

A star-shaped liquid crystal synthesized by connecting four cyanobiphenyl mesogens to the periphery of a super-hydrophobic and ultra-flexible cyclic siloxane ring with flexible hexyl chains formed the hierarchical layered superstructures.



HIERARCHICAL SUPERSTRUCTURE

**Crystalline Phase**   **SmA LC Phase**